Self-induced polarization anisoplanatism

James B. Breckinridge[1]
jbreckin@caltech.edu
California Institute of Technology
Pasadena, CA. 91106

ABSTRACT

This paper suggests that the astronomical science data recorded with low F# telescopes for applications requiring a known point spread function shape and those applications requiring instrument polarization calibration may be compromised unless the effects of vector wave propagation are properly modeled and compensated. Exoplanet coronagraphy requires "matched filter" masks and explicit designs for the real and imaginary parts for the mask transmittance. Three aberration sources dominate image quality in astronomical optical systems: amplitude, phase and polarization. Classical ray-trace aberration analysis used today by optical engineers is inadequate to model image formation in modern low F# high-performance astronomical telescopes. We show here that a complex (real and imaginary) vector wave model is required for high performance, large aperture, very wide-field, low F# systems.

Self-induced polarization anisoplanatism (SIPA) reduces system image quality, decreases contrast and limits the ability of image processing techniques to restore images. This paper provides a unique analysis of the image formation process to identify measurements sensitive to SIPA. Both the real part and the imaginary part of the vector complex wave needs to be traced through the entire optical system, including each mirror surface, optical filter, and all masks. Only at the focal plane is the modulus squared taken to obtain an estimate of the measured intensity.

This paper also discusses the concept of the polarization conjugate filter, suggested by the author to correct telescope/instrument corrupted phase and amplitude and thus mitigate[6], in part the effects of phase and amplitude errors introduced by reflections of incoherent white-light from metal coatings.

Keywords: Telescope optics, polarization, exoplanets, Lyot coronagraph, weak lensing, isoplanatism, internal polarization, image quality, polarization aberrations, geometric aberration, point spread function

1.0 INTRODUCTION

This paper introduces the concept of self-induced polarization anisoplanatism (SIPA) in telescopes, describes its origin and discusses its affects on science data. We describe how an optical system manipulates the complex (real and imaginary) vector wave through the telescope and instrument. The relationship between this wave and the system point spread function is discussed. We introduce the concept of the **complex point function** (CPF) defined as

$$PSF = |CPF|^2 = |a(x,y) + ib(x,y)|^2 \quad \text{Eq. 1}$$

where PSF is the well-known point spread function, and $a(x,y)$ is the coefficient on the real part of the electromagnetic field at the focus and $b(x,y)$ is the coefficient on the imaginary part of the complex field at the image plane.

[1] This work was partially funded by a grant from Breckinridge Associates, LLC , Pasadena, CA.

UV/Optical/IR Space Telescopes and Instruments: Innovative Technologies and Concepts VI,
edited by Howard A. MacEwen, James B. Breckinridge, Proc. of SPIE Vol. 8860, 886012
© 2013 SPIE · CCC code: 0277-786X/13/$18 · doi: 10.1117/12.2028479

The physics of image formation is described and the role of optical interference in the image formation process is described. Sources of polarization-induced anisoplanatism are identified, examples derived and the role of the complex (real and imaginary) vector waves is presented.

This paper is a continuation of our previous work[1,2,3,4,5,6] on the subject of physical optics vector wave propagation through a typical astronomical telescope optical system and the affects of this propagation on scientific astronomical data quality. In 2004, Breckinridge and Oppenheimer[3] showed that polarization introduced by image forming optics internal to a telescope & coronagraph optical system adds noise to the system and masks signatures important for the characterization of exoplanets. Optical coatings to control polarization in coronagraphs were discussed by Balasubramanian, et. al.[7] who suggested that coronagraphs may require a set polarization filters. Balasubramanian, et. al[8] addressed concerns about polarization throughout the visible and UV. In 2011, Clark and Breckinridge[6] proposed a birefringent polarization compensation window composed of birefringent optical nanostructures to correct for the Fresnel polarization aberrations and suggested a process for its manufacture, test and evaluation.

Isoplanatism is the optical scientists term to describe the behavior of the point spread function across the field of view, and through slight de-focus. The isoplanatic patch is defined as that small region (volume) in the focal plane where the image formation process is accurately represented as a process linear in intensity. This paper discusses analysis tools to calculate the magnitude of these effects.

2.0 REAL & IMAGINARY REFLECTIVITY

In this section we describe reflectivity for the real part of the field and reflectivity for the imaginary part of the field for a multi-element telescope. The notation is set for expressions in the remainder of the paper.

Figure 1 (below) shows two rays, one solid and one dashed originating at the same point on the object. These rays reflect from highly reflecting metal thin films coated onto mirror substrate surfaces 1 through 4. The optical power on these four optical elements is such that an image of the point on the object (plane 0) is imaged onto a region on the output plane 5. In this section, those terms related to the diffraction propagation of the wave fronts between surfaces will be ignored and we concentrate only on surface complex (real and imaginary) reflectivities.

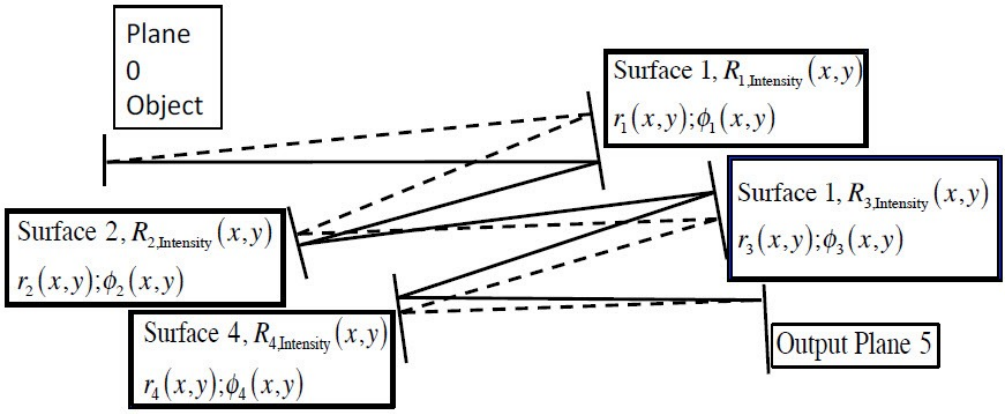

Figure 1 schematic of a 4-element optical system showing 2 rays: one dashed and the other solid propagating from plane 0 to plane 5. The rays originate from the same point on the object plane 0 and pass through the 4-element reflector system to the image or output at plane 5.

In Fig 1, we use R to represent the intensity reflectivity. The terms $r_n(x,y)$ are the amplitude of (real and imaginary) reflectivites of the complex wave at each surface n and the terms $\phi_n(x,y)$ are the reflectivity of the imaginary part of the complex wave. Each of the four surfaces in this figure is shown

with an **intensity** reflectivity $R_{n,\text{int}}$ where n is the surface number. The classical approach to the calculation of the intensity at output plane 5 is performed as shown in Eq. 2. Let $I_0(x,y)$ be the intensity in object space, then the intensity $I_5(x,y)$ in image space (plane 5) as a function of the intensity reflectivity of each surface is

$$I_5(x,y) = I_0(x,y)\prod_{i=1}^{4} R_{i,\text{int}} = I_0(x,y)\cdot R_{1,\text{int}}\cdot R_{2,\text{int}}\cdot R_{3,\text{int}}\cdot R_{4,\text{int}} \qquad \text{Eq. 2}$$

For most astronomical systems the calculation of the intensity at the focal plane using eq 1 is sufficient.

However, astronomical measurements that need high quality images and in-depth understanding of those images require analysis of the optical system in terms of the real and imaginary parts of the complex electromagnetic field as it reflects off each surface and passes through filters, lenses, beam-splitters and dispersing devices within the telescope and instrument system. Examples of such applications are coronagraphy for exoplanet characterization, precision focal plane metrology and precision polarization measurements. The SNR of these systems is particularly sensitive to the shape and stability of the point-spread function across the FOV.

There is a complex reflectivity Z at each surface *i*. Let

$$Z_i = r_i(x,y)\exp\left[i\phi_i(x,y)\right], \qquad \text{Eq. 3}$$

where $\phi_i(x,y)$ is the phase change introduced on the *i* th surface at the point *x,y* on that surface and $r_i(x,y)$ in the amplitude reflectance on the *i* th surface at the point *x,y* on that surface.

The transmittance for the entire system is then

$$Z_T(x,y) = \prod_{i=1}^{N} Z_i(x,y) = \prod_{i=1}^{N} r_i(x,y)\exp\left[i\phi_i(x,y)\right] \qquad \text{Eq. 4}$$

In Figure 1, let the field at the object plane 0 be represented as $U_0(x,y) = A_0\exp\left[i\phi_0(x,y)\right]$ and the field at the image plane 5 be represented by $U_5(x,y)$ then we find:

$$\left.\begin{aligned} U_5(x,y) &= A_0\exp\left[i\phi_0(x,y)\right]Z_T = \\ &= A_0\exp\left[i\phi_0(x,y)\right]\prod_{i=1}^{4} r_i(x,y)\exp\left[i\phi_i(x,y)\right] \end{aligned}\right\} \qquad \text{Eq 5}$$

In Fig 1 we show two rays passing through the system, one represented by a dashed line and the other represented by a solid line. If we use geometric ray trace to model and optimize the optical system, the computation adjusts element separation, tilt and surface curvatures to minimize the optical path difference (OPD) between the two rays, and indeed the entire family of rays that pass from the object to the image. In order to focus the energy onto the focal plane rays must strike at different points on mirror surfaces. Therefore, in general each ray reflects through a different angle at each surface.

We note that in Fig 1

1. Each ray strikes a different portion of each surface
2. Each ray that strikes a surface reflects through a different angle

We will use these facts in the development of the analysis for the self-induced polarization anisoplanatism (SIPA).

Details of the interaction of the complex (real and imaginary) wavefront with highly reflecting metal surfaces are given in Ch 13 of Born and Wolf[9]. In summary the values of the coefficients of the real part of the wave at the output plane 5, that is a_5 and the imaginary part of the wave at the output plane 5, that is b_5 depend on the geometric properties of the wave when it reflects from metal surfaces. Parameters include angle of incidence at a point on the surface of a reflecting element, as well as the real and imaginary parts of the index of refraction of the reflecting material. Manufacturing factors such as

contamination, electronic structure near the surface and metal thin film inhomogenieties (density) contribute to spatial variations in reflectivity.

A white-light incoherent unpolarized wave, common in astronomy will become partially polarized after reflecting from a metal surface (e.g. the primary mirror) and is further polarized after it strikes the next surface in the optical system and so on. The magnitude of this polarization depends on the angle the ray strikes each surface and, under some circumstances the point at which it reflects. For the curved optical surfaces needed to provide optical power for the telescope, the adjacent rays strike at different angles across the curved surface. In general, the steeper the angle the greater is the polarization.

The quality of the image is best if the polarization state is the same for all rays that strike the image plane to form a PSF. This is the same as saying that complex wave-fields are correlated. It is this correlation that enables the well-known unpolarized white-light fringe in interferometry. If the polarization state is not the same, a high quality image will not be formed. That radiation not contributing to the image will increase unwanted scattered light. Many astronomical sources of interest (exoplanets, reddened distant galaxies, nebulae) are intrinsically polarized. The polarized component of radiation from these sources interacts with the polarizing properties of the metal coatings on the mirrors to introduce radiometric and geometric errors that vary across the FOV.

Below, we show that in modern high-performance low F # astronomical optical systems, a geometric PSF, derived from the geometric ray trace will be a poor approximation to the PSF measured in an actual system. An understanding of the image quality requires an analysis of the associated vector complex wave with its real & imaginary parts to model the accuracy needed for modern high performance astronomical science.

3.0 THE POINT SPREAD FUNCTION (PSF)

In this section we describe the point spread function (PSF) of an optical system and discuss its utility as a metric of optical system performance[10,11]. Object space can be decomposed into an ensemble of points of light each point with its own characteristic optical amplitude and location in the field. This is shown schematically in Fig. 2.

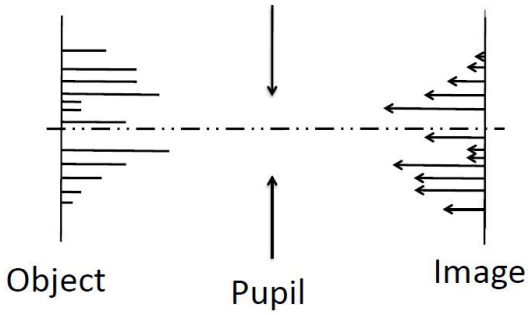

Figure 2 shows an object (left) decomposed into an ensemble of points (delta functions). The object field passes through the pupil to the image plane to the right. The pupil contains powered optical elements that convert the incoming diverging waves into converging waves that pass onto points in the image (right). The points at the right represent an intensity distribution across the focal plane and have all been broadened through convolution by the point-spread function (PSF).

The point-spread function (PSF) is the spatial frequency impulse response of a telescope-imaging system at a particular point in the field of view (FOV)[12]. It measures how well an object space point or area (point or ensembles of points) is mapped into image space. For an ideal optical system, each point in the object fills the telescope aperture (pupil) with a uniform complex electric field and each point in the image plane on the right "sees" a perfectly uniformly filled complex electric field when looking back from right to

left into the pupil. The PSF is in units of intensity. It is the modulus squared of the complex (real and imaginary) electromagnetic wave at the focal plane. Details of the shape and intensity of the PSF depends on how the "lens" at the pupil modifies the coefficient on the real term and the coefficient on the imaginary term in the electromagnetic field. In general the PSF is asymmetric, the shape changes across the FOV, and the shape will change with time depending on the mechanical stability of the system. The physical properties of the optical system deliver an electromagnetic field to the image plane. For a point in object space a complex point in image space is formed. This complex point function (CPF) is related to the point spread function as follows:

$$PSF = |CPF|^2 = |a(x,y) + ib(x,y)|^2 =$$
$$= \left| \delta_0(x_0, y_0) \exp[i\phi_0(x,y)] \prod_{i=1}^{4} r_i(x,y) \exp[i\phi_i(x,y)] \right|^2 \quad \text{Eq. 6}$$

A measure of the PSF does not provide information on how the image plane scale changes across the FOV, rather it is a metric of the local performance in a small region around a point on the object. That is, the PSF says very little about how the measured separation between two stars changes across the FOV. Aberration terms that model geometric projections are called distortion. These provide information on how the "plate" scale changes across the FOV.

4.0 PHYSICS OF IMAGE FORMATION

Optical systems of interest to astronomers, image in "quasi-monochromatic broadband white-light". Image formation is best understood as a phenomenon of the interference of converging electromagnetic waves described by two parameters one a real number and the other, an imaginary number[13].

Diffraction theory & the theory of interferometry provide tools to understand image formation. Figure 3 shows a schematic cross-section of an optical system reduced to its essentials. In Fig 3, plane 1, is the astronomical object; centered at plane 2 is the optical system shown here reduced to a simple bi-convex lens and to the right in the figure at plane 3 is the system focal plane where the detector is located. The horizontal line is the system axis.

The detector responds to the modulus squared of the complex real and imaginary electric field. We will give an expression to define the complex field at each plane within this simplified optical system then show the physical relationships between each plane and write an expression for the intensity or power at the focal plane. It is this intensity that is converted to electrons and recorded as a digital image of the scene.

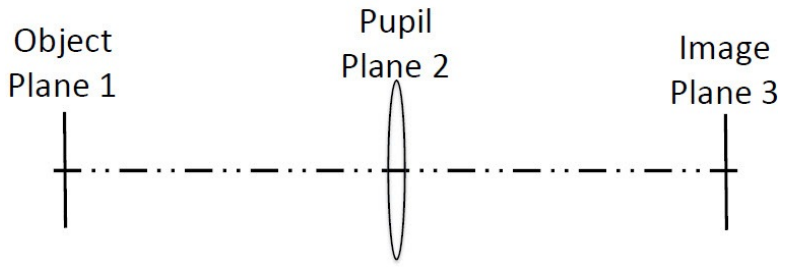

Figure 3 typical astronomical optical system reduced to its essentials. Plane 1 contains the object, plane 2 contains a powered optical element & defines the location of the pupil and plane 3 is the image plane. Radiation travels from the left to the right.

We will use orthogonal coordinates x, y to identify points on the object and image planes and orthogonal coordinates ξ, η to identify points on the pupil plane. The plus *z* direction is the direction of

propagation from left to right in Fig 3. The plane (*y, z*) of the drawing in Fig 3 is called the meridional plane by optical scientists and engineers.

We write the real, a and imaginary, b parts of the complex field $U_1(x_1, y_1)$ radiating from the object plane 1 as

$$U_1(x_1, y_1) = a_1(x_1, y_1) + ib_1(x_1, y_1) \quad \text{Eq. 7}$$

This complex field propagates from plane 1 to plane 2. Just to the left of the lens (the entrance pupil) located at the pupil plane 2 as shown in figure 3, we write the complex field as

$$U_2^-(\xi_2, \eta_2) = a_2(\xi_2, \eta_2) + ib_2(\xi_2, \eta_2) \quad \text{Eq. 8}$$

The complex field just to the left of the lens at pupil 2 is multiplied by the complex transmittance $T_2(\xi_2, \eta_2)$ of the lens. We then find the complex field just to the right of the lens at pupil plane 2 to be

$$U_2^+(\xi_2, \eta_2) = T_2(\xi_2, \eta_2)[a_2(\xi_2, \eta_2) + ib_2(\xi_2, \eta_2)] \quad \text{Eq. 9}$$

The complex transmittance of the pupil is written as,

$$T_2(\xi_2, \eta_2) = Z_2 = \prod_{i=1}^{N} Z_i = \prod_{i=1}^{N} r_i(\xi_2, \eta_2) \exp[i\phi_i(\xi_2, \eta_2)] \quad \text{Eq. 10}$$

where $r_i(\xi_2, \eta_2)$ represents the coefficient on the amplitude of the complex transmittance of the pupil and the coefficient $\phi_i(\xi_2, \eta_2)$ represents the coefficient on the imaginary part (phase) of the complex transmittance of the pupil.

In general the real part of the complex transmittance and the imaginary part of the complex transmittance of the pupil will be different for each point across the image plane. In an actual optical system there are many reflecting surfaces and windows few of which are at an actual pupil or image plane. To model the diffraction performance of these requires that we follow the real part of the complex wave separate from the imaginary part throughout the whole system and then take the modulus of the electric field at the focal plane to determine the intensity distribution at the focal plane.

The complex field just to the right of lens $U_2^+(\xi_2, \eta_2)$ at plane 2 is the exit pupil. The field is then propagated to plane 3, the image plane where the amplitude and phase of the complex field $U_3(x_3, y_3)$ is represented by

$$U_3(x_3, y_3) = a_3(x_3, y_3) + ib_3(x_3, y_3) \quad \text{Eq. 11}$$

The focal plane responds to intensity, or power (eg. Watts per cm^2) and the intensity across the focal plane is given by

$$I_3(x_3, y_3) = |U_3(x_3, y_3)|^2 = [U_3(x_3, y_3) U_3^*(x_3, y_3)] =$$
$$[a_3(x_3, y_3) + ib_3(x_3, y_3)][a_3(x_3, y_3) - ib_3(x_3, y_3)] = \quad \text{Eq. 12}$$
$$[a_3(x_3, y_3)]^2 + [b_3(x_3, y_3)]^2$$

Equation 12 shows us that the measured intensity at a point in the image plane is a function of both the amplitude (real part) and the phase (imaginary part) transmission properties of the optics. Figure 4 below contains a graphic that summarizes the notation we are using.

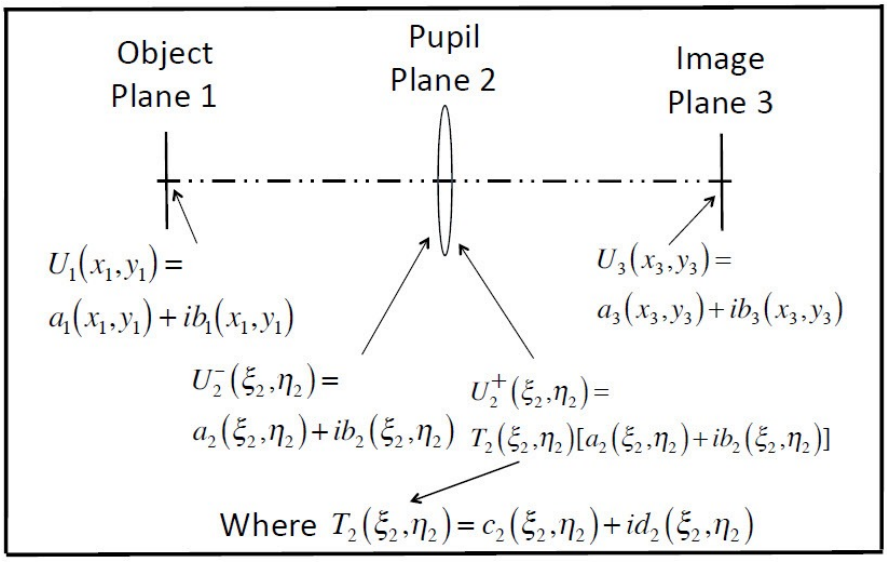

Figure 4 Summary of notation used in Eqs 7 through 12 and throughout this paper.

The Huygens-Fresnel principal and the Fresnel and Fraunhofer approximations show[14,15] that the intensity across the focal plane $I(x_3,y_3)$ as a function of the amplitude and phase at the exit pupil $U_2^+(\xi_2,\eta_2)$ is given by integrating the complex field over the exit pupil and taking the modulus squared of the field (amplitude and phase) at the image plane after integration:

$$I_3(x_3,y_3)=A^2\left|\int_{-\infty}^{\infty}\int_{-\infty}^{\infty}U_2^+(\xi_2,\eta_2)\exp\left[-i\frac{2\pi}{\bar{\lambda}f}(x_3\xi_2+y_3\eta_2)\right]\right|^2 d\xi_2 d\eta_2 \qquad \text{Eq. 13}$$

The term

$\exp\left[-i\frac{2\pi}{\bar{\lambda}f}(x_3\xi_2+y_3\eta_2)\right]$ represents the powered optical element which modifies the phase curvature of the incoming complex (real and imaginary) wavefronts so they converge to points (e.g. (x_3,y_3) across the image plane.

In Eq. 14 $\bar{\lambda}$ is the mean weighted wavelength under the conditions that $\bar{\lambda}/\Delta\lambda \gg 1$ (quasimonochromatic assumption) and f is focal length. A is a scaling factor.

The complex amplitude and phase term $U_2^+(\xi_2,\eta_2)$ in Eq. 13 contains information about both the science object and the telescope pupil. If the object-space distribution is a point source in the field at plane 1 in Fig 4 at the off axis at position x_0,y_0, then, $U_1(x_1,y_1)=\delta[x_1-x_0,y_1-y_0]$. The field just in front of the pupil is a tilted plane wave. In this situation, the complex amplitude and phase term $U_2^+(\xi_2,\eta_2)$ in Eq. 13 contains only information about the telescope pupil and the angle position (x_0,y_0) in object space. It is this telescope pupil amplitude and phase that tells us the point spread function at plane 3 in Fig 4, for different points across the field of view.

If we examine figure 4 within the framework of equations 9 and 13, we see there are 2 cases to consider:

1. If $U_2^+(\xi_2,\eta_2) = \begin{cases} 1 \text{ inside the aperture} \\ 0 \text{ otherwise} \end{cases}$

then the imaging system has no phase $b(\xi,\eta)$ or amplitude $a(\xi,\eta)$ aberrations and the performance of the system is diffraction limited. This characterizes the perfect, ideal optical system and is not realizable in the practice.

2. If $U_2^+(\xi_2,\eta_2) \neq \begin{cases} 1 \text{ inside the aperture} \\ 0 \text{ otherwise} \end{cases}$

then the imaging system has phase errors and amplitude errors or both and the performance of the system is less than ideal, perhaps undesirable and does not meet requirements.

In this case the complex transmittance of the pupil, as given in Eq. 9 by $T_2(\xi_2,\eta_2) = c_2(\xi_2,\eta_2) + id_2(\xi_2,\eta_2)$ is not $T_2(\xi_2,\eta_2) = 1.0 + i0.0$, as we would find in a perfect optical system (case 1 above). The term $c_2(\xi_2,\eta_2)$ represents the changes in real part of the of the complex transmittance across the pupil (ξ_2,η_2) and the term $d_2(\xi_2,\eta_2)$ represents changes in the imaginary part of the transmittance at point (ξ_2,η_2).

The point-spread function (PSF) is the modulus squared of the complex (real and imaginary) electric field at the focal plane for a point source in object space. The function is not limited to an on axis point, but also is used to describe the system performance across the field of view. The PSF for an on axis point is found by placing a point source modeled as: $\delta(x_1,y_1)$. This point source propagates to the entrance pupil at plane 2. A point source is unresolved, therefore the field $U_2^-(\xi_2,\eta_2)$ is uniform. Therefore from Eq. 10, we see that

$$U_2^+(\xi_2,\eta_2) = T_2(\xi_2,\eta_2) \qquad \text{Eq 14}$$

From equation 13, we see that the complex field at the image plane is given by the integral expression inside the mod-squared term. This expression is known to be the Fourier transform with real and imaginary parts of the field $U_2^+(\xi_2,\eta_2)$ and therefore, by Eq 15, the real and imaginary part of the Fourier Transform of $T_2(\xi_2,\eta_2)$, the function that characterizes the pupil. Under these conditions then,

$$PSF = \left| \mathcal{F}\left\{ T_2(\xi_2,\eta_2) \right\} \right|^2$$

Therefore the PSF is a metric of the optical system intensity performance and not the complex amplitude and phase performance. It is the latter that both provides an important diagnostic tool as well as information tneeded to design an optimum Lyot mask. It is one of many metrics needed to constrain the system requirements.

The next section shows that the image formation process is an interference phenomenon and that the best image quality requires that the complex electromagnetic wave from all regions on the pupil be coherent at the focal plane. Later, we

examine a typical astronomical telescope and identify physical sources of errors on the real part of the complex wave and physical sources of errors in the imaginary part of the complex wave. In a later section, we identify methods to mitigate these effects. In the next section we show how image formation is an interference phenomenon, review the role of partial coherence in image formation and examine the role of instrument-induced polarization in image quality.

5.0 IMAGE FORMATION IS AN INTERFERENCE PHENOMENON

Image formation is a phenomenon of interference. Consider the image quality at a point on the image plane. Stand at that point on the focal plane and look back out through the telescope to object space with an eye that is sensitive to both phase and amplitude. If all regions of the pupil interfere with all of the other regions, then the integral shown in Eq. 13 above is uniformly weighted across the pupil. A metric of the degree to which there is good interference from waves across the pupil is fringe contrast or the visibility of fringes. If radiation from a region on the pupil interferes with radiation from all the other regions on the pupil, then we have good quality imaging at that point. An additional way of thinking about this is that for each field point at the image plane, all regions across the pupil are coherent with all of the other regions to give good high-contrast image quality. Interference fringes reveal the degree of coherence[16,17] between electromagnetic fields. If the fields are orthogonally polarized, for example then no interference or image formation takes place and the unused radiation contributes to scattered light corresponding to a decrease in contrast and poor SNR for exoplanet detection and characterization.

Consider a perfect optical system with a uniformly illuminated in phase and amplitude circular exit pupil and no amplitude or phase aberrations. That is, in Eq. 11 the term

$$T_2\left(\xi_2,\eta_2\right)\equiv 1.0 \text{ that is } \left[c_2\left(\xi_2,\eta_2\right)=1.0 \text{ and } d_2\left(\xi_2,\eta_2\right)=0.0\right].$$

Radiation from all portions of the pupil will interfere equally. In this case, for a uniformly illuminated pupil, the PSF is given by the well-known Bessel function:

$$I(\theta)=I_0\left[\frac{2J_1(r)}{r}\right]^2 \qquad \text{Eq. 15.}$$

To demonstrate that image formation is an interference phenomenon,we now take this circular aperture, divide it in half and cover each half with two sheets of linear Polaroid as shown in Figure 5. On the left in this figure we see that the left half of the exit pupil is covered with a linear polarizer that transmits in the vertical direction and that the right half is covered with a linear polarizer that transmits in the horizontal direction. Radiation from the left half of the pupil will not interfere with the radiation from the right half. The wavefronts between the two regions in the pupil are not correlated. The apertures resemble two letter D, one facing to the right and the other facing to the left. The left hand side pupil is said to be incoherent with respect to the right hand side pupil. This will also be the case for orthogonally circular polarized pair of sheets shown on the right of the figure below.

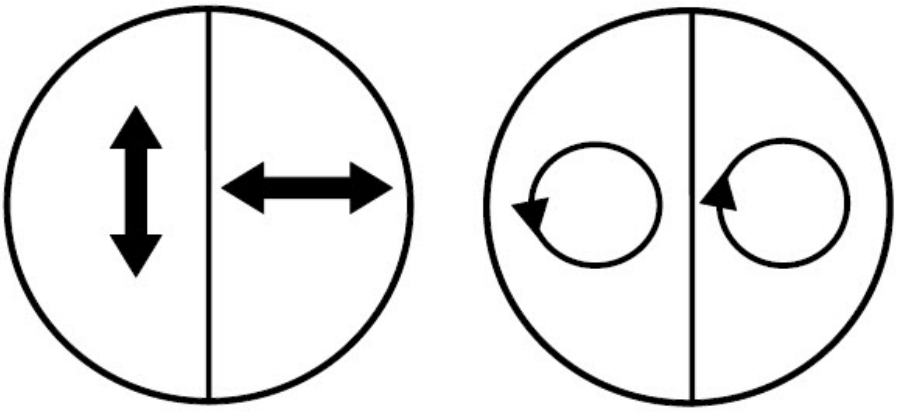

Figure 5. Left shows the exit pupil of a telescope with orthogonal linear polarizers placed over the pupil. Right shows the exit pupil of a telescope with orthogonal circular polarizers placed over the pupil.

The resulting PSF at the image plane is then the simple linear (not vector) sum of two PSF's rotated back to back. Each is a PSF characteristic of a filled D-shaped aperture, rather than the PSF for filled circular aperture that is representative of the perfect telescope pupil and shown in Eq. 15. Instrumentally induced polarization in actual telescope/instrument systems is not usually 100% but partially polarized often with different degrees of polarization across the wavefront. This partially polarized light, which does not interfere changes the weighting of the terms in the integral shown in Eq. 13, changes the symmetry of the PSF, increases scattered light and reduces the scene contrast so very important for exoplanet coronagraphy.

Radiation that does not interfere does not contribute to the image formation process but does contribute to the increase in the background and the uniformity of that background. This reduction in contrast is extremely important in stellar coronagraphy where scene contrast levels as high as 10^{+11} are desired.

Of course, in an actual telescope/instrument system an astronomer would not insert a polarizer to intentionally degrade the performance of his system. However, any surface in the entire optical path that introduces partial polarization, either circular or linear will distort the PSF and will increase scattered light. Optical filters, diffraction gratings[18], fold mirrors[19,20] needed for packaging, and the necessary powered optical elements[21] to control geometric aberrations introduce internal polarization to modify the PSF. Such polarization induced aberration needs to be understood in detail to optimize the detection and characterization of exoplanets using coronagraphy and astrometry. The author is actively persuing research in this area.

An example of how highly reflecting metal thin film polarization alters the on-axis PSF is understood by examining figure 6 below. Here we show 4 rays labeled A, B, C and D passing through a lens and coming to a focus at point P to the right. A flat mirror is used to reflect the converging beam so that it comes to a focus at point P'. Most modern space optical systems require a flat mirror located in a converging beam in order to fit or package the optical system into a spacecraft.

Breckinridge and Oppenheimer[3] show that for an F# 1.5 primary mirror, 13% of the radiation from the annulus near the rim will be linearly polarized with radial preference. This jumps to over 22% for a system like WFIRST-2.4 which has an F#=1.2.

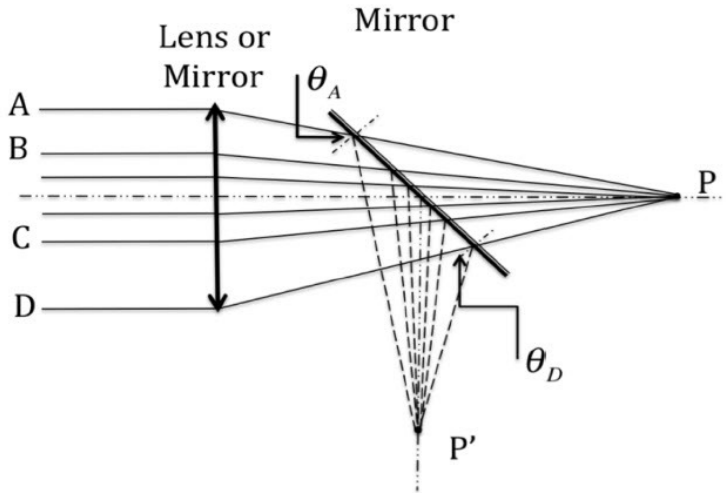

Figure 6. The ray bundle ABCD is shown passing from the left to the right. The rays originate in an optical system off the drawing to the left. The ray bundle strikes a fold mirror and converges to an on-axis focal point P'.

Figure 6 shows a portion of an optical system in the vicinity of a fold mirror typically required to package the optical system for spaceflight. To maintain a high reflectivity telescope, mirrors are typically a highly reflecting metal coating placed on a dielectric substrate. Radiation from the left has been collected by a low F# large primary mirror and thus is partially polarized across the complex wavefront (real and imaginary part) ABCD. The degree of partial polarization is, in general different for each ray in the cluster ABCD. The complex wavefront that enters the system from the left has a varying polarization content across its surface.

The flat mirror is shown intercepting a converging complex (real and imaginary part) wavefront whose normals are represented by the rays shown. Let ray AP' have an angle of incidence on the mirror represented by θ_A and let ray DP' have an angle of incidence on the mirror represented by θ_D. From figure 6, we see that $\theta_A > \theta_D$. We find a taper or an apodization caused by polarization (polarization apodization) across the pupil as viewed from point P' and the on-axis point spread function will be distorted. Portions of the wavefront are not mutually coherent, do not contribute to the image formation process and increase unwanted radiation.

In this section we have shown that the elements of complex (real and imaginary part) wavefront at the focal plane are partially polarized. Orthogonal polarization states do not interfere. Consequently the on axis PSF is asymmetric. In a Lyot coronagraph, an optimum Lyot mask placed at this focus needs to be a matched amplitude and phase (real and imaginary) filter mask to maximize the probability for the detection and characterization of exoplanets.

In the next section we analyze the propagation of a complex wave through a typical optical system and identify hardware that contributes to sources of errors in the real and imaginary parts of the wavefront.

6.0 PROPAGATION THROUGH A TYPICAL TELESCOPE

In this section, we review the Fresnel equations and examine in detail those aspects of a typical astronomical telescope that are responsible for errors in the ideal shape of the PSF. The coefficients on the real and imaginary parts of the complex wave are examined in detail. Specific terms in the expression: $\left[T_2(\xi_2,\eta_2) = c_2(\xi_2,\eta_2) + id_2(\xi_2,\eta_2)\right]$ are examined in detail in the following sections where we consider several physical sources of error that cause the ideal PSF to be asymmetric and to have unwanted structure.

6.1 Polarization content changes on reflection: Fresnel equations

A highly reflecting metal mirror in an optical system is a partial polarizer. The absorption coefficient for light polarized parallel is different that that for the radiation polarized perpendicular to the plane of

incidence. In addition there will be a phase change between the wavefronts created by the two different polarizations. Starlight with no preferential polarization will become partially polarized upon reflection at the F#=1.2 primary mirror. This partially polarized complex wave will reflect from additional metal mirrors as it passes through the optical system, to further polarize the wavefront. The degree of polarization at points across the wavefront is determined by the real and imaginary parts of the index of refraction of the metal mirror and any dielectric stack overcoat as well as the angle the rays strike the surface.

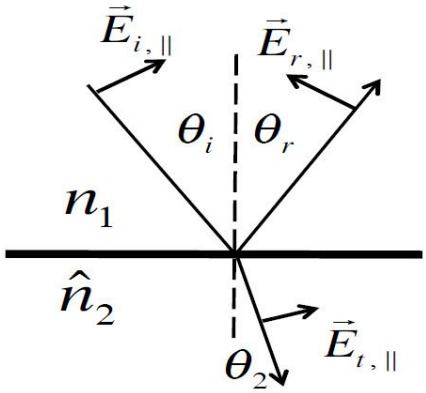

Figure 7 a ray representing a normal to the complex (real and imaginary) optical wavefront strikes a metal mirror and reflects. The amplitudes characteristic of the ray are changed as is the phase to introduce a small circular polarization component.

The complex reflectivities $r_\perp$ and $r_\parallel$ change across the surface of a curved mirror, are dependent on the field point and depend on the real and imaginary parts of the index of refraction. We can represent them by:

$$\left.\begin{aligned} r_\perp &= f\left(\xi_2,\eta_2;x_1,y_1;n,k\right) \\ r_\parallel &= f\left(\xi_2,\eta_2;x_1,y_1;n,k\right) \end{aligned}\right\} \qquad \text{Eq. 16}$$

Since the index of complex refraction in the metal depends on the polarization and the absorption is wavelength dependent, there is a wavelength dependent phase shift upon reflection. This phase shift can be represented by

$$\phi_{\parallel-\perp} = f\left(\xi_2,\eta_2;x_1,y_1;n,k\right). \qquad \text{Eq. 17}$$

Details on how this calculation is made is found in several references[22,23]. The equations are lengthy and will not be repeated here to save space.

The reflectance is different for each polarization and we can write

$$\left.\begin{aligned} \left[T_{\perp,\mathcal{F}}\left(\xi_2,\eta_2;x_1,y_1;n,k\right) = c_{\perp,\mathcal{F}}\left(\xi_2,\eta_2;x_1,y_1;n,k\right) + id_{\perp\mathcal{F}}\left(\xi_2,\eta_2;x_1,y_1;n,k\right)\right] \\ \left[T_{\parallel\mathcal{F}}\ \left(\xi_2,\eta_2;x_1,y_1;n,k\right) = c_{\parallel\mathcal{F}}\ \left(\xi_2,\eta_2;x_1,y_1;n,k\right) + id_{\parallel\mathcal{F}}\left(\xi_2,\eta_2;x_1,y_1;n,k\right)\right] \end{aligned}\right\} \qquad \text{Eq 18}$$

Where we have used a script F to indicate those terms calculated using the real and imaginary parts of the index of refraction based on the Fresnel equations for metals.

6.2 Sources of amplitude (real part) errors

This section examines three sources of pupil errors that contribute to the amplitude, $r_i(\xi_2,\eta_2)$ in Eq. 11

6.2.1 Secondary and its support mask the primary

With the exception of Schmidt telescope type configurations and the Schwartzchild configuration, the stop (and thus the entrance pupil) of an astronomical telescope is always located at the largest (and thus most expensive) optical element. Most astronomical telescopes today have obscured apertures. Figure 8 below shows amplitude transmittance for a Cassegrain as viewed from the image plane looking back toward object space. The drawing on the left is for an on-axis point and the drawing on the right is for a point in the field, in the 4th quadrant of the image plane. For Cassegrain telescopes the secondary support system cannot be located at the primary mirror. For off axis field points the shadow of the secondary its support systems on the primary are displaced from the hole in the primary mirror as shown on the right.

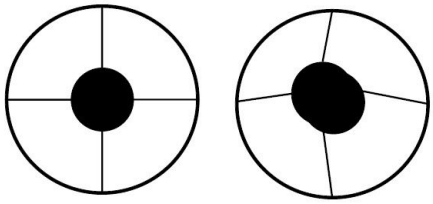

Figure 8 shows the ξ_2,η_2 plane for a pupil as viewed from a point on axis (left) and for the same pupil as viewed from a point off axis. Note that the term $r_i(\xi_2,\eta_2)$ changes as we move across the field of view because the secondary mirror housing and the secondary support structure vignettes different portions of the exit pupil as a function of FOV. Note that this error is binary, that is, regions on the pupil are either on (open) or off (closed).

The fact that the pupil on the left is not identical to that on the right means that the term $U_2^+(\xi_2,\eta_2)$ in Eq. 13 changes as a function of the point in the FOV, and the shape of the PSF therefore changes across the FOV. The mask function amplitude transmittance depends on location in the field of view *x,y*. The mask function can be represented by the expression:

$$T_{mask} = mask(x_1,y_1;\xi_2,\eta_2) \qquad \text{Eq. 19}$$

6.2.2 Area projection at the pupil

The amplitude (real) transmittance across the pupil depends on the F# of the primary mirror. The theoretically perfect PSF for a circular aperture assumes a uniformly illuminated aperture. However the amplitude transmittance changes because the primary mirror and other optical elements in the system are curved to provide optical power.

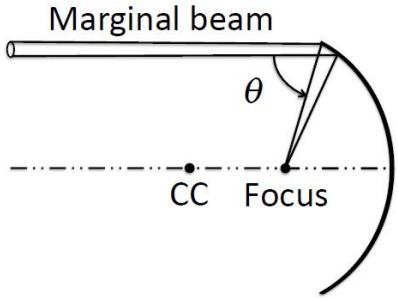

Figure 9 A cross-section view a typical telescope in the meridional plane showing the center of curvature (CC), the focus and the marginal beam for a concave primary mirror. The marginal beam is shown striking the edge of the pupil and deviating through angle θ to the focus.

Large aperture space telescopes are typically of low F# because of the mechanical-structural constraints required by packaging a telescope for launch. F#'s as low as 1.2 are not unusual for designs of

modern space telescopes. The angle, θ, that the marginal beam (shown in Fig 9) deviates when it reflects from the curved telescope entrance aperture (pupil) is given by

$$\theta = \arctan\left[\frac{1}{2F^{\#}}\right] \qquad \text{Eq. 20}$$

where θ is the angle of deviation of the marginal ray at the edge of the pupil. To find the ideal PSF (Eq. 15), which gives intensity at the image plane, we assume a uniformly illuminated pupil, not one that tapers to the edge. That is, we assume that the power per unit area (Watts/M^2) was constant across the pupil to obtain Eq. 15. From the geometry in Fig 9 we see that the power per unit area on the pupil as viewed from the image plane drops off as we move from the center to the edge. The power per unit area reflected decreases across the radius of the pupil. At the edge of the pupil the radiation per unit area is decreased by a factor of $\cos\left[\frac{\theta}{2}\right]$ compared to the center. The larger the surface area, the more power to the focal plane. The outer annulus of the mirror contributes the most power and therefore this projection angle is important.

This small effect is ignored in typical telescope applications, which do not need high quality imaging with low F#'s telescope primaries. For those astronomical applications studied here this is important. In polar coordinates the transmittance is then

$$T_2(\theta_2,\phi_2) = \propto \cos\left[\frac{\theta}{2}\right] \qquad \text{Eq. 21}$$

where the angle used in this equation is defined in Fig 9.

For a wide field of view system, the angle θ depends on field of view in addition to the location of the intercept point on the pupil, and the effective reflectivity becomes

$$r(x_1,y_1;\xi_2,\eta_2) = \rho\cos\frac{\theta(x_1,y_1;\xi_2,\eta_2)}{2} \qquad \text{Eq. 22}$$

where ρ is the pupil reflectivity at normal incidence.

Note that in off-axis systems there are no obscurations like those shown in Fig. 6. But the angle θ, shown in Fig 9 remains and the PSF is distorted differently across the FOV depending on FOV position.

6.2.3 Reflectivity variations across the surface of large area optical thin films

The highly reflecting coating deposited on large area telescope mirrors has small changes in reflectivity across the surface with a characteristic spatial correlation, not unlike the term r_0 used to describe atmospheric turbulence in ground-based adaptive optics. Local variations in reflectivity between 90 and 97% are not uncommon[24]. The effects of these variations on image quality is generally not taken into consideration in current models. The real part of the amplitude transmittance is then represented by

$$\tilde{T}_2(\xi_2,\eta_2) = \sum_{i=1}^{N}\tilde{\rho}(\xi_i,\eta_i;x_0,y_0) \qquad \text{Eq. 23}$$

where $\tilde{\rho}$ represents samples from a random variable that is characteristic of the variations in normal incidence reflectivity across a large primary mirror, generally ranging between 0.97 and 0.92.

6.3 Sources of phase (imaginary part) errors are carried in the term: $\phi_i(\xi_2,\eta_2)$ in Eq. 11.

6.3.1 Optical surface errors

No telescope mirror can be fabricated perfectly. The optical figuring process polishes the correct macroscopic figure onto the mirror, but leaves small figure errors that affect image quality. Wavefront errors are unintentionally polished into the front surface of the primary mirror. Control of these errors becomes more difficult as the F# decreases. Indeed the current state of the art is about F#=1.2 and the best surface is about 50 nm RMS[25].

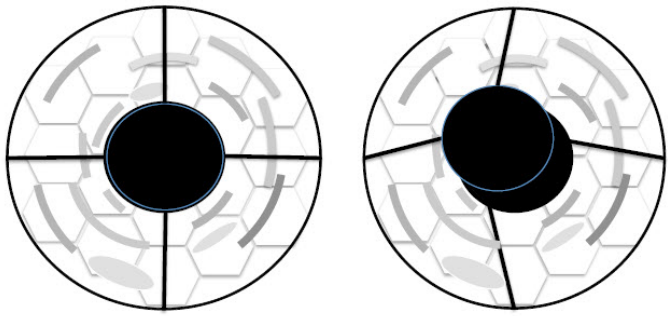

Figure 10 shows the ξ_2, η_2 plane for a pupil as viewed from a point on axis (left) and for the same pupil as viewed from a point off axis (right). The gray portions represent optical surface figure errors and we can see a print-through of the hex pattern typical of large telescope mirrors.

Here we consider only phase terms, we write $r_i(\xi_2, \eta_2) = 1.0$ and we have:

$$\phi_t(\xi, \eta) = \sum_{i=1}^{N} \phi_i(\xi, \eta) \qquad \text{Eq 24}$$

The relationship that models the transfer of the complex wave-front from the pupil to the image plane is given by Eq. 13, which is repeated below.

$$I_3(x_3, y_3) = A^2 \left| \int_{-\infty}^{\infty} \int_{-\infty}^{\infty} U_2^+(\xi_2, \eta_2) \exp\left[-i \frac{2\pi}{\bar{\lambda} f} (x_3 \xi_2 + y_3 \eta_2) \right] \right|^2$$

In Fig 10, we note that the phase coefficient $\phi = (\xi, \eta)$ changes as we move across the field of view because the secondary mirror housing and the secondary support structure vignettes different portions of the wavefront aberrated exit pupil depending on the observers location in the FOV. This causes an anisoplanatism.

The term $U_2^+(\xi_2, \eta_2)$ changes across the FOV. Since the shape of the PSF is determined by integrating the complex function (real and imaginary) across the pupil as shown in Fig 10, a measure of the PSF at one point in the field will not accurately represent the PSF at another part of the FOV.

6.3.2 Parallel and perpendicular phase reflectivities

Unpolarized light is often thought of as an ensemble of randomly oriented polarized beams. The reflection process filters this ensemble of beams to produce a partially polarized reflected beam. For light polarized in the vertical that strikes a metal mirror at a non-zero incidence angle has its amplitude decreased by a factor of $(A_r / A_i)_{\|}$ and phase changed upon reflection by a factor $(\varphi_r / \varphi_i)_{\|}$. For light polarized in the

horizontal that strikes a metal mirror at a non-zero incidence angle has its amplitude decreased by a factor of $\left(A_r / A_i\right)_\perp$ and phase changed upon reflection by a factor $\left(\varphi_r / \varphi_i\right)_\perp$. We find then

$$\left.\begin{array}{c} \left(A_r / A_i\right)_\parallel \neq \left(A_r / A_i\right)_\perp \\ \text{and} \\ \left(\varphi_r / \varphi_i\right)_\parallel \neq \left(\varphi_r / \varphi_i\right)_\perp \end{array}\right\} \qquad \text{Eq. 25}$$

7. Polarization anisoplanatism

Image restoration for astronomers is discussed in Ch 9.13 in the book: Basic Optics for the Astronomical Sciences[26]. The isoplanatic region is that area over the focal plane where the PSF remains the same. The system diffraction PSF derived from the star image is used to restore the aberrated image to near the diffraction limit. The mathematical process is similar to that used in speckle interferometry[27,28] An example of isoplanatism is shown in Fig 5 of the paper by Breckinridge, McAlister and Robinson[29]

An astronomical telescope with low F#, and thus a polarized complex (real and imaginary) wavefront with additional mirrors in the system will suffer from polarization anisoplanatism.

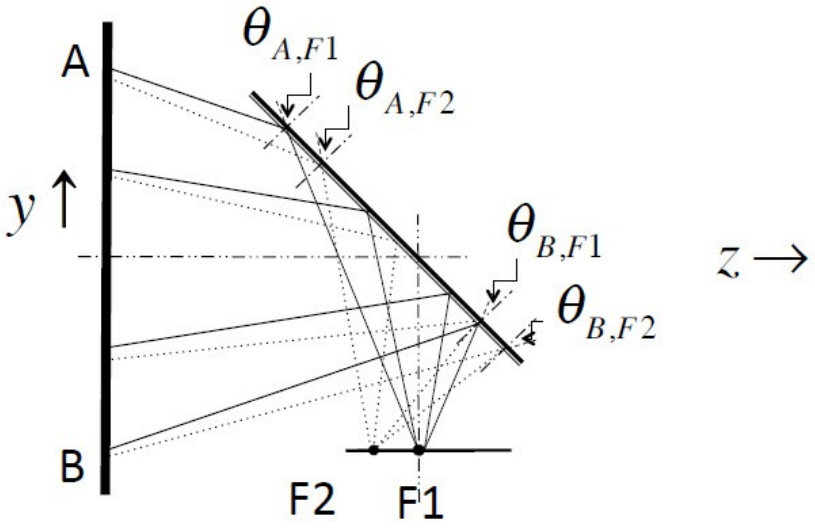

Figure 11 The ray bundles A & B are shown passing from a large aperture telescope to the left to strike a fold mirror and then come to a focus. Note there are two field points. One is indicated by F1 and the other is indicated by F2.

Figure 11 shows a portion of an optical system in the vicinity of a fold mirror typically required to package the optical system for spaceflight. To maintain a high reflectivity telescope, mirrors are typically a highly reflecting metal coating placed on a dielectric substrate. Radiation from the left has been collected by a low F# large primary mirror and thus is partially polarized, with the degree of polarization changing across the complex wavefront (real and imaginary part) $\overline{A}\overline{B}$. The complex wavefront that enters the system from the left has a varying polarization content across its surface.

In Figure 11 we represent the wavefront by 4 rays, which are normal to the surface of the wavefront. Each ray has a different polarization content. The flat mirror is shown intercepting a converging complex (real and imaginary part) wavefront. Consider two field points. One is on axis and shown as F1.

The other is off axis and in the field and is shown as F2. Let the ray BF1 have an angle of incidence on the mirror represented by $\theta_{B,F1}$ and let ray BF2 to the other field point F2 have an angle of incidence on the mirror represented by $\theta_{B,F2}$. Let ray AF1 have an angle of incidence on the mirror represented by $\theta_{A,F1}$ and let ray AF2 to another field point have an angle of incidence on the mirror represented by $\theta_{A,F2}$.

From this Figure 9, we can see that $\theta_{B,F1} \neq \theta_{B,F2}$ and that $\theta_{A,F1} \neq \theta_{A,F2}$ and the polarization content of the complex (real and imaginary part) of the field at point F1 is not the same as that at plane F2. Therefore the PSF at point F1 is not equal to that at point F2 and F2 is said to be outside the isoplanatic region of F1.

The geometric ray trace assures that the optical path difference (OPD) is optimized to minimize geometric spot sizes at points F1 and at F2 in the field. This implies that the wavefront phase errors are minimized. However, because there are metal thin films in the powered optical system and in fold mirrors the reflectivity for that part of the incident white light that is polarized horizontal to the plane of incidence is not equal to that for the component polarized vertical to the plane of incidence. Some regions of the wave front that combine to form the image are incoherent with other regions. Interference does not take place to contribute to an image and that radiation contributes to background to reduce contrast.

8. Corrector plate to compensate for the Fresnel Reflections in on-axis systems

Breckinridge[30] suggested that a Fresnel polarization aberration corrector be designed and built to mitigate the effects of the Fresnel polarization aberrations. A test plan is written, materials to fabricate the device have been identified and the fabrication process defined. We are waiting for funding.

9. Summary, recommendations and conclusions

Polarization anisotropy in low F# telescopes needs further analysis. The polarization complex field transfer function is under development to accurately assess the performance of those NASA science missions that require very high fidelity image quality.

Acknowledgements

The author would like to acknowledge very helpful conversations with K. Patterson of CALTECH and with Prof. Chipman of the College of Optical Sciences, University of Arizona and Bob Breault of BRO optical.

References

[1] Breckinridge, J. B. "Polarization Properties of a Grating Spectrograph," Applied Optics, 10, 286-294 (1971).
[2] Breckinridge, J. B. "Diffraction Grating Polarization," IAU Col. 23, Tucson, "Planets, Stars, and Nebulae Studied with Photo-Polarimetry", T. Gehrels (ed.) (1973).
[3] Breckinridge, J. B. and B. Oppenheimer, "Polarization Effects in Reflecting Coronagraphs for White Light Applications in Astronomy," Ap J, 600, pp 1091 – 1098 (2004).
[4] J. B. Breckinridge, "Image Formation in High Contrast Optical Systems: The role of polarization." Proc. SPIE 5487 page 1337-1345 (2004).
[5] Joseph Carson, Brian Kern, James Breckinridge, John Trauger "The effects of instrumental elliptical polarization stellar point spread function fine structure" Proc IAU Colloquium No. 200: Direct Imaging of Exoplanets: Science and Techniques. Pages 441 to 444 (2006).
[6] Clark, N. and J. B. Breckinridge "Polarization compensation of Fresnel aberrations in telescopes", Proc. SPIE **81460O**, 1 to 12 pages (2011)
[7] Balasubramanian, K., D. J. Hoppe, P.Z.Mouroulis, L. F. Marchen and S. B. Shaklan "Polarization compensating protective coatings for TPF-Coronagraph optics to control contrast degrading cross polarization leakage" Proc SPIE **5905** 59050H-1-11 (2005)

[8] Balasubramanian, K., S. Shaklan, A. Give'on, E. Cady, L.Marchen "Deep UV to NIR space telescopes and exoplanet coronagraphs: a trade study on throughput, polarization, mirror coating options and requirements". (2011)
[9] Born M and E. Wolf, "Principles of Optics", 6th ed Pergamon Press Ch 13 (1993)
[10] Gaskill, Jack D., "Linear systems, Fourier transforms and Optics", John Wiley and Sons, pages 335 & 406, (1978)
[11] Gross, Herbert, "Handbook of Optics Vol 2", Wiley VCH pages 208, 217, 275 (2005)
[12] Breckinridge, J. B. "Basic Optics for the Astronomical Sciences", SPIE press page 200, section 9.11 "Optical Transfer Function" (2012)
[13] Breckinridge, J. B., "Basic Optics for the Astronomical Sciences", Ch 10. SPIE Press, Bellingham WA. (2012).
[14] Born M and E. Wolf, "Principles of Optics", 6th ed Pergamon Press (1993) Ch 10
[15] Goodman, J. W., "Introduction to Fourier Optics" Roberts and Company, Greenwood Village, Co. (2005)
[16] Wolf, Emil, "Introduction to the Theory of Coherence and Polarization of Light", Cambridge University Press, (2007)
[17] Reynolds, G. O. , J. B. DeVelis, G. B. Parrent and B. J. Thompson (1989) "The new physical optics notebook: Tutorials in Fourier Optics", SPIE and American Institute of Physics.
[18] Breckinridge, J. B. "Diffraction Grating Polarization"**,** IAU Col. 23, Tucson, *Planets, Stars, and Nebulae Studied with Photo-Polarimetry*, T. Gehrels (ed.). (1973)
[19] McGuire, J. and Chipman, R. "Polarization aberrations. 2. Tilted and decentered optical systems", Applied Optics **33**, 5101, (1994)
[20] McGuire, J. P. and R. A. Chipman (1994) "Polarization aberrations 1. Rotationally symmetric optical systems", Appl. Opt. 33, (1994).
[21] Breckinridge, J and B. Oppenheimer "Polarization effects in reflecting coronagraphs for white-light applications in astronomy", ApJ **600**, 1091 (2004)
[22] Clarke, David, "Stellar Polarimetry" Wiley VCH Verlag GmbH & Co. KGaK pp 381 (2010)
[23] Knittl, Zdenek, "Optics of Thin Films" John Wiley & sons (1976)
[24] Gary Matthews, Excelis private communication (2013)
[25] Gary Matthews, Excelis, Private communication (2013)
[26] J. B. Breckinridge "Basic Optics for the Astronomical Sciences", 418 page text. SPIE Press, Bellingham, WA. (2012)
[27] Weigelt, G., "Triple-correlation imaging in optical astronomy", Progress in Optics **29**, 293-319, (1991)
[28] Alloin, D. M., and J.-M. Mariotti, "Diffraction limited imaging with very large telescopes", NATO ASI series, Kluwer Academic Publishers, Dordrecht, Boston & London, (1988).
[29] J. B. Breckinridge, H. A. McAlister and W. G. Robinson, "The Kitt Peak Speckle Camera." Applied Optics, 18, 1034-1041, (1979).
[30] Clark, N. and J. B. Breckinridge "Polarization compensation of Fresnel aberrations in telescopes", SPIE Proc. 8146-0O, 1 to 12 pages (2011).